PHOTOEMISSION CURRENT AND SOLAR EUV RADIATION: CLUSTER AND TIMED OBSERVATIONS

Anders I. ERIKSSON and Erik WINKLER

Swedish Institute of Space Physics, Uppsala, Sweden, and
Department of Astronomy and Space Physics, Uppsala University, Sweden

Solar EUV radiation causes photoemission from conductors in space. We compare measurements of photoelectron emission from the EFW instruments on the Cluster satellites to solar EUV data from TIMED/SEE for the years 2003-2006. Comparing the variations (solar rotation, annual, solar cycle) of the two quantities, we can study the photoelectron yield function that should relate them. We find that no yield function can give perfect agreement between the data sets, but that reasonable correspondence is achieved by the photoelectron yield of pure Al. We also show that taking solar EUV variations into account when calibrating spacecraft potential data for use as a density measurement significantly increases the accuracy.

1. INTRODUCTION

In tenuous plasmas, emission of electrons from a spacecraft exposed to ultraviolet (UV) radiation by the photoelectric effect is a major feature of the spacecraft-plasma interaction. In sufficiently tenuous plasmas, the spacecraft becomes positively charged in order to maintain current continuity. In these tenuous plasmas, ion currents are small, and the only other source of current is the plasma electrons. The fewer such electrons there are available, the higher potential must the spacecraft attain in order to drag back a sufficient part of its emitted photoelectrons [1, 2]. This is because the photoelectrons will have a distribution decreasing with increasing energy, often assumed to be Boltzmannian.

The spacecraft potential can be estimated from Langmuir probe bias voltage sweeps [3, e.g.] or from the voltage of probes fed with bias current [4, e.g.]. The latter case is often the more convenient, as this provides a continuous measurement and is a natural by-product of electric field measurements by double-probe instruments [5]. The quantity directly measured is the probe-to-spacecraft potential V_{ps}, which has usually assumed to differ from $-V_{\mathrm{S}}$ only by the small voltage drop over the probe sheath. While recent simulations by Cully et al. [6] shows that this is normally not true because the electrostatic potential from the spacecraft has usually not decayed fully at the location of the probe, the relation between V_{S} and V_{ps} will still be linear to good approximation. We can therefore use V_{S} and V_{ps} interchangeably. The method to use V_{ps} as a density proxy therefore works well in practice, where one usually calibrates the $n(V_{\mathrm{ps}})$ relation using observations in a region where n can be determined by other means [4, 7, 8, 9].

As the basis for this method is the balancing of the electrons carried to and from the spacecraft by photoemission and plasma electron collection, respectively, it is clear that the conversion of V_{ps} measurements to density estimates must depend on the solar UV flux. To investigate this relation is the primary task of this study. In Section 2, we expand the qualitative arguments above to show how the UV flux enters the density-V_{ps} relation. To experimentally study the UV influence on spacecraft photoemission, we combine photoemission saturation current determinations from the EFW instruments on the Cluster satellites with UV spectra from TIMED/SEE in Section 3. We go on to see the effect of compensating for UV flux variations in Section 4, and finally summarize our results in Section 5.

2. GENERAL CONSIDERATIONS

The electrostatic potential of a spacecraft with respect to the surrounding plasma, V_S, is determined by the requirement that all currents to the spacecraft must add up to zero. In many cases, it is sufficient to consider three current sources: the currents due to capture of plasma electrons and ions, denoted I_e and I_i, respectively, and the current due to emission of photoelectrons, I_f. It is conventional to define currents as positive when flowing from the spacecraft to the plasma, so I_e is positive while I_i and I_f are negative. The exact expressions for how these currents depend on V_S will vary with spacecraft geometry and plasma regime (dense/tenuous, magnetized/unmagnetized, subsonic/supersonic flow, etc), but it is always possible to define a characteristic magnitude for each of these. For I_e, the characteristic magnitude is normally the thermal (or random) electron current [10],

$$I_{e0} = A_e ne \sqrt{\frac{KT_e}{2\pi m_e}} \tag{1}$$

where A_e is the effective electron collection area of the spacecraft, n is the electron number density, e is the electron charge, KT_e the characteristic electron energy in the plasma and m_e is the electron mass. A similar expression often applies to the ions, with obvious substitutions of parameters relevant for the ions, though in the common case of supersonic ion flow with respect to the spacecraft, the relevant characteristic ion current obviously is

$$I_{i0} = A_i neu, \tag{2}$$

where A_e is the effective ion collection area of the spacecraft (basically the cross section in the flow direction) and u is the plasma flow speed in the spacecraft frame of reference. The more complicated case of ion flow speed of same order as the ion thermal speed, treated by e.g. Medicus [11, 12] and Hoegy and Brace [13], is still possible to formulate in terms of these characteristic currents. Finally, the photoelectron current has a characteristic magnitude

$$I_{f0} = A_f \int Y(\lambda) F(\lambda) \, d\lambda \tag{3}$$

depending on the ultraviolet (UV) flux F at each wavelength λ as well as on the photoelectron yield function $Y(\lambda)$ of the spacecraft surface material [14]. The effective photoemission area A_f is the area of the spacecraft projected to the UV source, usually the sun.

From the viewpoint of spacecraft-plasma interactions, one may reasonably define a plasma as *dense* when I_{f0} is small compared to the two other currents, which in practice will mean that it is small compared to I_{i0}, which always is much smaller than I_{e0}. If $I_{i0} \ll I_{f0}$ but $I_{e0} \gtrsim I_{f0}$ we may similarly classify the plasma density as *intermediate*, while the plasma is *tenuous* if $I_{e0} < I_{f0}$. In the last case, the spacecraft potential will be positive. At Earth orbit, supersonic ion flow is common (typical for any spacecraft in the ionosphere or solar wind, for example, and actually also in the magnetotail lobes [15, 16]), and typical values of u and I_{f0}/A_f are a few km/s and a few tens of μA/m^2, respectively [17, 14, 4]. Using equation (2), we thus find that terrestrial plasmas are dense in this sense when the plasma density is some 10^4 cm^{-3} or higher. The limit for where the plasma is tenuous in this sense will vary with the electron energy, but may typically be around 100 cm^{-3}. In the tenuous and intermediate cases, the equilibrium spacecraft potential will be given by the relation

$$I_e(V_S) + I_f(V_S) \approx 0. \tag{4}$$

As $I_e(V_S)$ depends on n, we see that for stationary UV emission, it is possible to derive the plasma density from a measurement of V_S. As the density of a tenuous plasma is difficult to determine by other means but is fundamental to know for understanding space plasmas, this observation has formed the basis of the very useful density measurement method discussed in Section 1.

Different functional forms for $I_{e,i,f}(V_S)$ may apply in different circumstances. However, two general and reasonable physical requirements are that the currents will all be growing functions of V_S, i.e.

$$\frac{dI_{e,f,i}}{dV_S} \geq 0, \tag{5}$$

and that they all go to zero in one limit: I_e as $V_S \rightarrow -\infty$, I_i and I_f as $V_S \rightarrow +\infty$. These assumptions alone lead to positive (negative) spacecraft potentials in sufficiently tenuous (dense) plasmas. If we write the electron current as

$$I_e = I_{e0}\, g(V_S) = n\, h(V_S), \tag{6}$$

and the photoemission current as

$$I_f = -I_{f0}\, f(V_S), \tag{7}$$

the density is found from observed V_S by use of (4) as

$$n = \frac{I_e(V_S)}{h(V_S)} = -\frac{I_f(V_S)}{h(V_S)} = I_{f0}\frac{f(V_S)}{h(V_S)}. \tag{8}$$

Why this exercise? The important point is that Equation (8) shows that any error in our knowledge of I_{f0} will propagate to an equal error in the density estimate n. But as I_{f0} depends lineary on the UV flux (Equation (3)), it is clear that any conversion of spacecraft potential to plasma density aiming to be accurate over a time period so long that the UV flux can change appreciably must include some measure of the UV flux. In the next Section, we investigate the variations of I_{f0} and UV flux, and return to the influence of the UV flux on the $n(V_S)$ relation, or equivalently the $n(V_{ps})$ relation which is what is actually established from measurements, in Section 4.

3. PHOTOEMISSION DATA ANALYSIS

3.1 Photoemission measurements

To determine the photoemission saturation current I_{f0}, we use the probe bias voltage sweeps regularly performed by the Electric Fields and Waves (EFW) instruments [18] on each of ESA's four Cluster satellites [19].
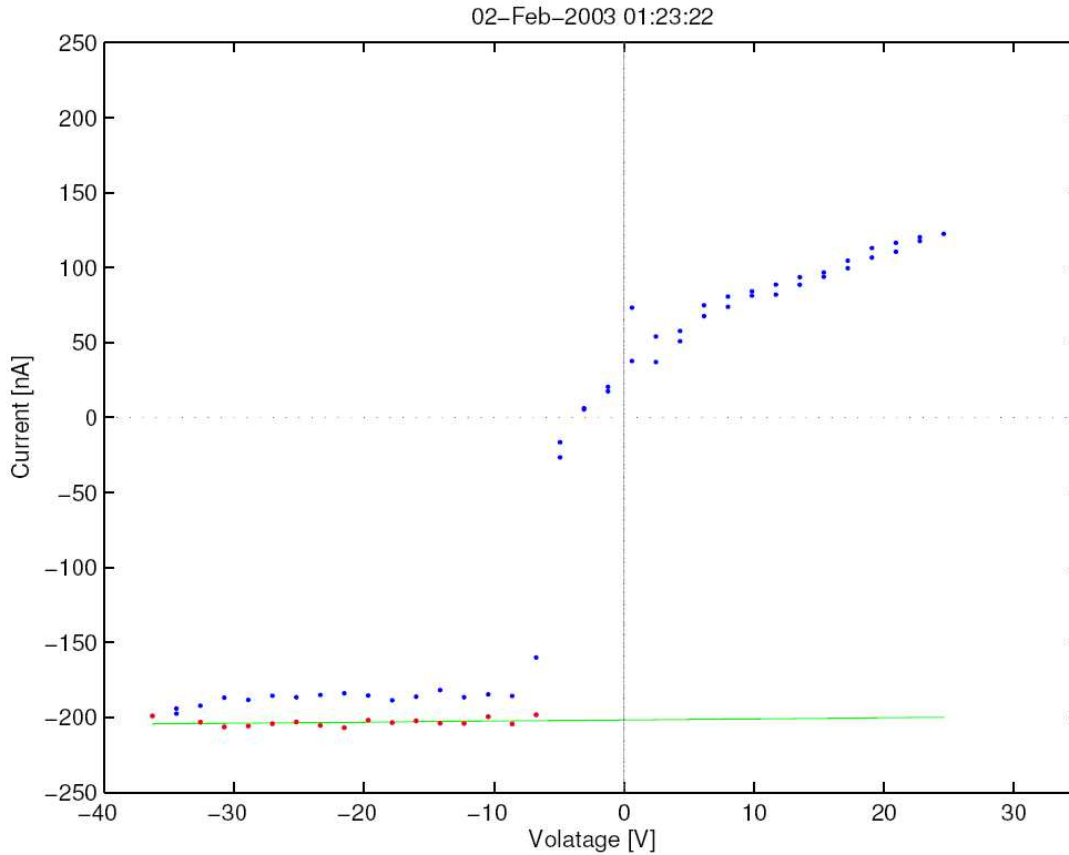

Fig. 1. A probe bias voltage sweep from Probe 2 of the EFW instrument on Cluster spacecraft 3, acquired on February 2, 2003, at 01:23:22 UT.

The EFW probes are aluminium spheres of radius 40 mm, covered by a conductive Aquadag coating intended to provide uniform photoemission properties. They are mounted on the tips of four wire booms extending 44 m from the spacecraft spin axis, forming a symmetric cross in the spin plane. The spin rate is close to 15 rpm. An example probe voltage bias sweep is shown in Figure 1. Such sweeps are obtained on average once every four hours for all operational EFW probes. Each sweep takes less than a second and is really a double sweep: the bias potential is first varied from max negative to max positive value and then back again. The red data points in Figure 1 show the data points used for determining the photoelectron saturation current I_{f0}, which are all from the later (downsweeping) part of the sweep. The apparent difference in photoemission for the upsweep and the downsweep is due to different spin phase: while the probe as such is symmetric, it is connected to a thin (diameter 0.5 mm) wire connecting it to the thicker wire boom 1.5 m away. This makes the photoemitting surface of the probe vary by almost 10% during the spin, but as each sweep is started at the same spin phase angle with respect to the sun by use of the sun pulse from the onboard solar sensor, this will not be a problem for our statistics as long as we stick to using the same part of the sweep all the time. We have chosen the downsweep part.

The green line shows a least squares fit to the red points, almost flat as expected for a probe at negative potential with respect to the surrounding plasma and all photoelectrons are driven away. For automatic extraction of I_{f0} from the sweeps, we used an algorithm [20] based on finding the "knee" of the sweep, i.e. the bias voltage below which the current is flat and representing I_{f0}, by use of the continuous V_{ps} values obtained around the sweep. Additional criteria on stability, outliers, small risk of ion current contamination etc. were applied, and we restricted ourselves to the period 2003-2006, when comparison UV data from TIMED were available (Section 3.2) and Cluster/EFW sweeps were obtained regularly. As the total database is large (around 100,000 sweeps available for the years $2003 – 2006$) we could apply rather strict criteria on the data and still get a useful statistical sample: some 10,000 sweeps remained to give photoemission estimates. The resulting time series, smoothed with a 3-day moving average filter, for EFW probe 2 on Cluster 3 is shown as the blue points in the upper panel of Figure 2. We will return to the further details of this figure later on.

3.2   Solar UV measurements

Since its launch in December 2001, the SEE instrument on NASA's TIMED satellite (sun-synchronous orbit, 625 km altitude) is the best available continuous provider of solar UV data [21]. We have used the standard data product (available at CDAWweb), which gives one UV wavelength spectrum, obtained during a few minutes time once each TIMED orbit, in 1 nm bins from 1 nm to 194 nm. As there is no synchronization between Cluster/EFW sweeps and TIMED/SEE spectral measurements, we have interpolated and made 3-day running averages. Data can therefore be presented on a common time line, but to actually compare the two data sets, we need a means to relate them. This is provided by the yield function introduced in Equation (3). Yield functions for the materials of interest for the EFW probes, aluminium and Aquadag, have been published by Samson and Cairns [22] and Feuerbacher and Fitton [17]. These functions are shown in the lower plot of Figure 2.

When these yield functions are convolved with the TIMED/SEE UV spectra according to Equation (3), we get the red (aluminium) and green (DAG-213) curves in the upper panel of Figure 2. The yield measured for aluminium has been increased by around 10% to better fit the actually measured probe current (blue data points in upper panel). This increase can be motivated by the actual increase of the photoemitting area electrically connected to the probe due to the thin wire (Section 3.1). With this increase, we can see that the measured photosaturation currents and the values we calculate from TIMED and the aluminium yield function match rather well. One can clearly see in the data the same variations, on a short period corresponding to the solar rotation, on an annual scale due to the variation of distance to the sun, and the declining trend of the solar cycle. Higher values around the "Halloween storms" of October-November 2003 are also clearly detectable in both data sets. However, there are also features that do not fit between the data sets. In general, there is a tendency in the data derived from the UV data to show a higher amplitude of the short-term (solar rotation) fluctuations than do the actually measured data. In addition, the UV-derived data give lower values than the EFW photocurrent measurements for early 2003, while the opposite is true for mid-2006. These differences are systematic and similar between all 14 operational EFW probes, but their causes yet remain to be explained.
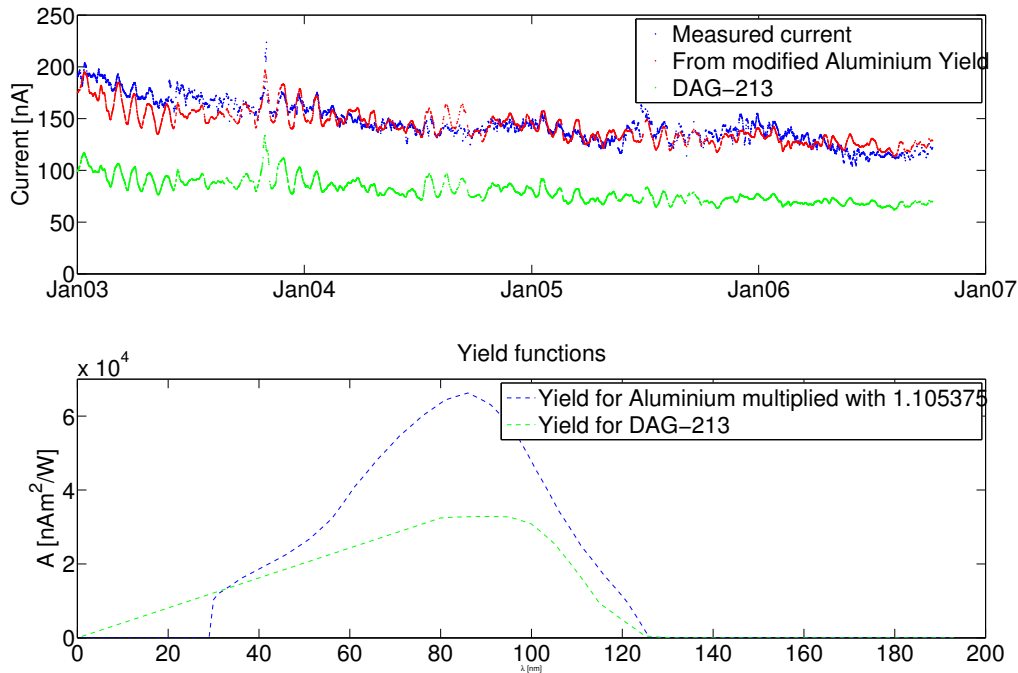
Fig. 2. *Upper panel:* The photoemission saturation current as measured by Cluster/EFW probe number 2 on Cluster spacecraft 3 (blue) and calculated from TIMED/SEE UV data using a yield function for aluminium (red) and DAG-213 (green). *Lower panel:* The yield functions used. The yield function for DAG-213 has been linearly extrapolated by us below 80 nm.

It is of interest to note that the UV-derived data for Aquadag has nowwhere as good an agreement with probe photosaturation current measurements as do the data based on the aluminium yield profile. Increasing also this yield function by 10% would help somewhat but not solve the problem. This might be taken to imply that the Aquadag coating is not very stable in space and could wear off on a timescale of a year, or that the Aquadag layer is so thin that it has little impact on the photoemission. However, more work remains to do before any final conclusion can be drawn. It is not clear that the tested materials are fully equal to the Cluster samples, and one should also note that the Aquadag measurements are significantly older than the aluminium data and ends artificially at 80 nm, below which we have extrapolated them. Nevertheless, the matter deserves investigation.

3.3 Deriving yield from satellite data

Is there a way to determine the actual yield function from the probe current and solar UV data? If so, this would have the possibility to determine this property of the probe surface material which might help for studying its evolution. It would also have the potential to find a yield function without the problems of reproducing the data in smallest detail that we discussed above. Can we find such a function?

Formally, the answer is yes. Approximate the integral in Equation (3) by a sum. Given a large set of probe currents and solar UV spectra, we have a linear system of equations. The system is probably overdetermined, but we can solve it in a least squares sense. However, the yield function must be restricted to positive values, a restriction not likely to result from an ordinary least squares method. We therefore used the LSQNONNEG algorithm, which restricts solutions to positive values [23]. However, the attempt was not very succesful, as can be seen in Figure 3. While the calculated photoemission in the upper panel (red) reasonably follows the measured values (blue) in some average sense, the agreement is hardly any better than in Figure 2. Some aspects are worse, i.e. the exaggeration of solar rotation period signals. But more important is that the yield function, shown in the lower panel, is physically unrealistic: all emission is concentrated into a few peaks.

To derive the yield function in Figure 3, we used all data from all probes on all spacecraft, 2003–2006. If
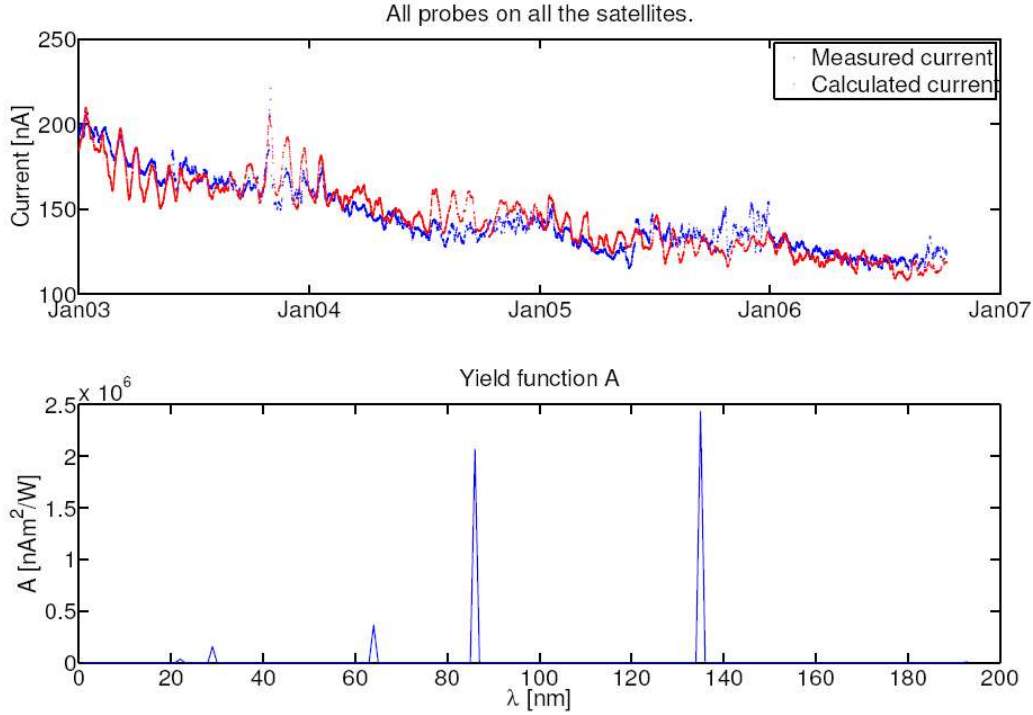
Fig. 3. *Upper panel:* The photoemission saturation current as measured by Cluster/EFW probe number 2 on Cluster spacecraft 3 (blue) and calculated from TIMED/SEE UV data using a yield function determined from all probes on all Cluster satellites, shown in the lower plot.

restricting to some subset of the data, the non-negative least squares fit still picks out only a few wavelengths as non-zero, but the wavelengths it picks will be different for each subset. This is a natural behaviour of the algorithm on noisy data, further illustrating the unphysical nature of the result. The attempt to optimize the yield function in this way thus failed.

4. COMPENSATING V_{ps} DENSITY ESTMATES FOR VARYING UV

4.1 Relation of density to V_{ps} in the solar wind

To empirically study the influence of varying UV flux on the $n(V_{ps})$ relation we have compared the Cluster/EFW V_{ps} data to density data obtained by the ClusterIon Spectrometer (CIS) instrument [24, 25] in the solar wind. We restricted the study to Cluster 3 and data for February-March for the years 2003-2006. In this period, we identified solar wind intervals manually using the CSDS web plots, available at http://www.cluster.rl.ac.uk/. We only used intervals where CIS ran the HIA sensor in a mode optimized for solar wind measurements. For V_{ps} as well as CIS density, we used the spin resolution data available in the Cluster Science Data System (CSDS) [26]. This resulted in some 1.1 million data points (spins), plotted as a two-dimensional histogram in the left panel of Figure 4. The points clearly lines up very well in this log-log-diagram, showing a quite well defined $n(V_{ps})$ relation, which we will now seek to further improve.

4.2 Compensating for UV variations

The data presented in Section 3.2 clearly showed the covariation of the photosaturation current I_{f0} with the solar UV emissions. According to Equation 8, the relation $n(V_{ps})$ must then also depend on the UV flux, and we should try to compensate for this.

What is the best measure of solar UV for this purpose? The most obvious candidate must be our measurment of I_{f0} itself (Section 3.1), as I_{f0} is the quantity actually turning up in Equation (8). We could also think of using the photoemission current as derived from the TIMED/SEE UV spectra and an assumed photoelectron yield function, as in Section 3.2, though that would restrict the use of our results to the period since TIMED
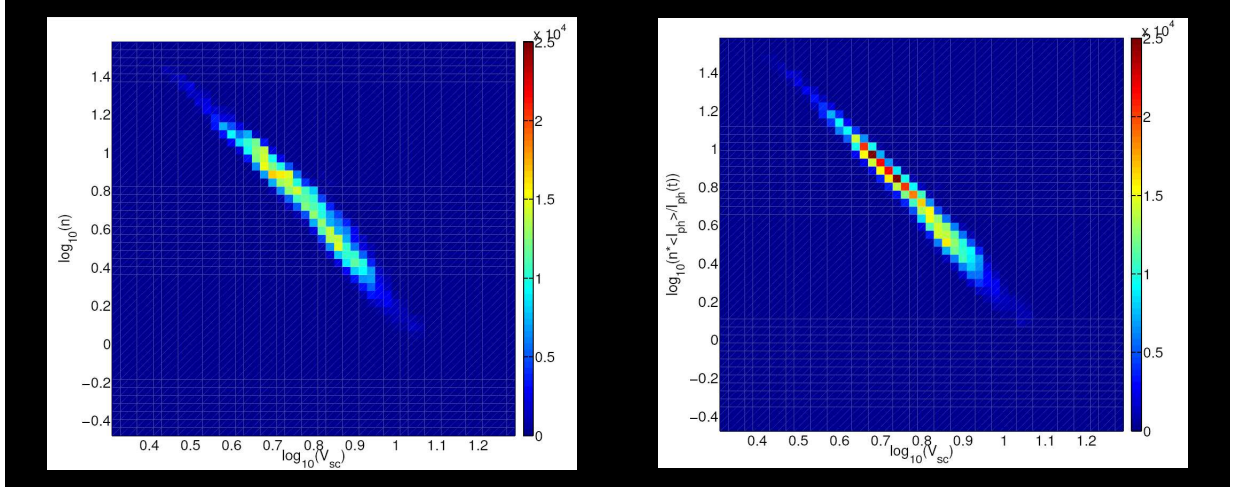
Fig. 4. Two-dimensional histograms of solar wind plasma density from Cluster/CIS and probe-to-plasma potential from Cluster/EFW, all from Cluster 3 for the months February-March in the years 2003-2006. In the right panel, the density data have been compensated for the varying photoemission current. The colour coding is number of points per bin: the total number of data points is around 1.1 million.

became operational. Another idea is to use a solar UV proxy, in order to extend the possible use of the method to periods before the launch of TIMED. A simple and often used solar UV proxy is the intensity of the 10.7 cm solar radio emission line. This quantity, known as $F_{10.7}$ or F10.7, has been measured daily since 1948 and is easily available. More refined UV proxies can be constructed from F10.7 and/or other data, for instance from UARS [27]. An example is the E10.7 index [28], but for its simplicity and wide availability, we here use F10.7, which has a reasonable correlation with the integrated TIMED/SEE UV flux on long time scales as can be seen in Figure 5.

We thus constructed two compensated density measures,

$$n_{\mathrm{I}}(t) = \frac{< I_{\mathrm{f0}} >}{I_{\mathrm{f0}}(t)} n(t) \qquad (9)$$

and

$$n_{\mathrm{F}}(t) = \frac{< F_{10.7} >}{F_{10.7}(t)} n(t) \qquad (10)$$

where the brackets denote time averaging. From the point of view of using V_{ps} as a density proxy, it may seem backward to normalize the density in this way, but the idea here is only to see the influence on the spread of data points of such a normalization. The idea is that we would first establish a relation of the form $n_{\mathrm{I}}(V_{\mathrm{ps}})$, apply this to V_{ps} data, and finally get a good estimate of the real density as a function of time by inversion of (9).

The first of these compensated densities, n_{I}, is plotted versus V_{ps} in the right panel in Figure 4. Comparing to the raw data in the left plot, it seems clear that the points now align better, with less spread perpendicular to the approximate line on which they almost line up. To quantify this impression, we calculated linear least-squares fits for each of the plots, and looked at the root mean square deviation of the points from this line in the vertical (log density) direction. The result is 0.99 for the raw data n, 0.87 for F10.7-compensated data n_{F} (not plotted), and 0.81 for current-compensated data n_{I}. The impression that the spread is reduced in the right panel of Figure 4 is thus quantitatively verified. Interestingly, even F10.7, which is a rather inexact UV proxy, signficantly reduces spread, though it is likely to introduce severe errors for some individual data points (note the outliers in the lower panel of Figure 5).

5. CONCLUSIONS

In this study, we have undertaken two related investigations: to study the covariation of the photoemission data from Cluster/EFW with the UV spectra from TIMED/SEE, and to investigate a method for improving the use
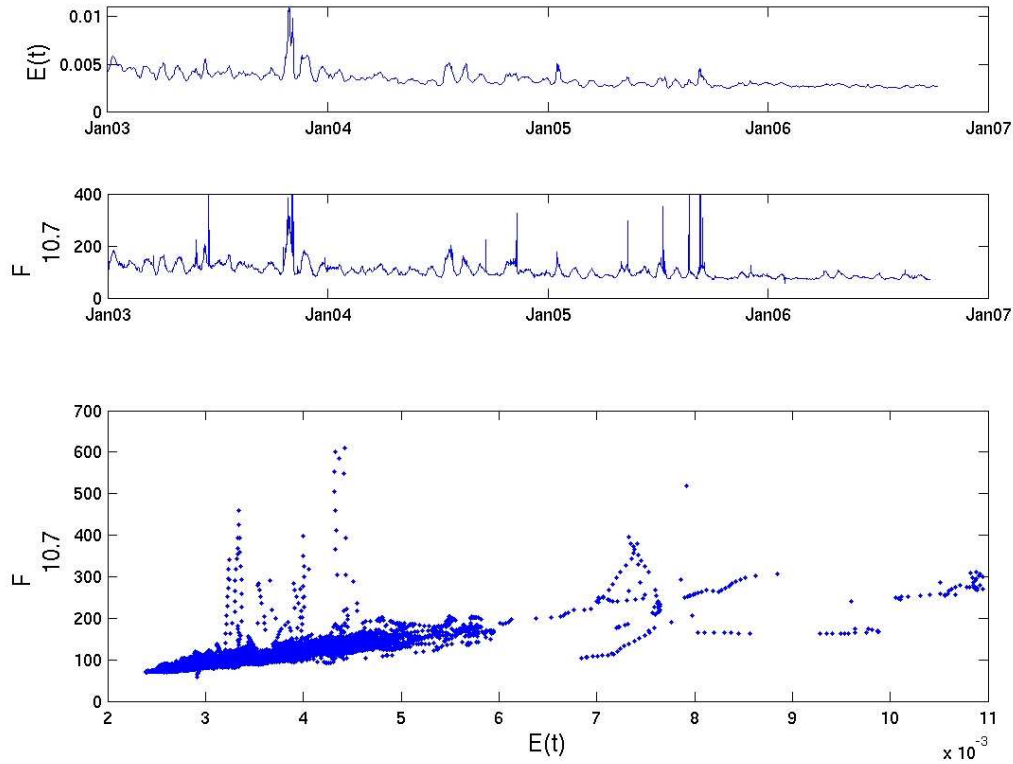
Fig. 5. Time series of the integrated TIMED/SEE UV flux (upper panel) and the F10.7 index (centre panel), and a scatter plot of the two quantities.

of V_{ps} data as a denity proxy by compensating for UV flux variations. Comparing photoemission currents from Langmuir probes to EUV measurements is not new: a good example is the Pioneer Venus Orbiter investigations by Brace et al. [29], which have been used as a measure of the integrated solar UV flux [30]. However, the availability of daily UV spectra as well as Langmuir probe data, both obtained around the same planet, makes the dataset we have used unique.

1) The photoemission current determined from Cluster/EFW probe bias sweeps correlate well but not perfectly with UV flux measurements from TIMED/SEE.

2) The photoelectron current calculated from TIMED/SEE data and laboratory photoelectron yield for aluminium reproduces the observed current well.

3) Laboratory photoelectron yield for the original probe coating (Aquadag) only gives around 60% of the observed photoemission. The reason for this reamins to investigate.

4) The use of spacecraft potential as a proxy for plasma density can be improved by correcting for UV flux variations. Even a rough UV proxy like F10.7 significantly reduces the data spread.

Acknowledgements

References

[1] E. C. Whipple. *The equilibrium potential of a body in the upper atmosphere and in interplanetary space*. PhD thesis, George Washington University, 1965.

[2] P.-A. Lindqvist. The potential of ISEE in different plasma environments. In *Proc. of the 17th ESLAB Symp. on Spacecraft/Plasma Interactions and their Influence on Field and Particle Measurements, Noordwijk, The Netherlands, ESA SP-198*, pages 25–33. European Space Agency, 1983.

[3] J.-E. Wahlund, R. Boström, G. Gustafsson, D. A. Gurnett, W. S. Kurth, A. Pedersen, T. Averkamp, G. B. Hospodarsky, A. M. Persoon, P. Canu, F. M. Neubauer, M. K. Dougherty, A. I. Eriksson, M. W. Morooka, R. Gill, M. André, L. Eliasson, and I. Müller-Wodarg. Cassini measurements of cold plasma in the ionosphere of Titan. *Science*, 308:986–989, 2005.

[4] A. Pedersen. Solar wind and magnetosphere plasma diagnostics by spacecraft electrostatic potential measurements. *Ann. Geophysicae*, 13:118–129, 1995.

[5] A. Pedersen, F. Mozer, and G. Gustafsson. Electric field measurements in a tenuous plasma with spherical double probes. In J. Borovsky, R. Pfaff, and D. Young, editors, *Measurement Techniques in Space Plasmas: Fields (AGU Geophysical Monograph 103)*, pages 1–12. American Geophysical Union, 1998.

[6] C. Cully, R. E. Ergun, and A. I. Eriksson. Electrostatic structure around spacecraft in tenuous plasmas. *J. Geophys. Res.*, accepted for publication, June 2007.

[7] C. P. Escoubet, A. Pedersen, R. Schmidt, and P. A. Lindqvist. Density in the magnetosphere inferred from ISEE 1 spacecraft potential. *J. Geophys. Res.*, 102:17595–17610, 1997.

[8] A. Pedersen, P. Decreau, P. Escoubet, G. Gustafsson, H. Laakso, P.-A. Lindqvist, B. Lybekk, F. Mozer, and A. Vaivads. Four-point high time resolution information on electron densities on Cluster. *Ann. Geophys,*, 19:1471–1481, 2001.

[9] H. Laakso. Variation of the spacecraft potential in the magnetosphere. *J. Atm. Solar-Terr. Phys.*, 64:1735–1744, 2002.

[10] H. M. Mott-Smith and I. Langmuir. The theory of collectors in gaseous discharges. *Phys. Rev.*, 28:727–763, 1926.

[11] G Medicus. Theory of electron collection of spherical probes. *J. Appl. Phys.*, 32:2512–2520, 1961.

[12] G. Medicus. Spherical Langmuir probe in drifting and accelerated Maxwellian distribution. *J. Appl. Phys.*, 33:3094–3100, 1962.

[13] W. R. Hoegy and L. H. Brace. Use of Langmuir probes in non-Maxwellian space plasmas. *Rev. Sci. Instr.*, 70:3015–3024, 1999.

[14] R. J. L. Grard. Properties of satellite photoelectron sheath derived from photoemission laboratory studies. *J. Geophys. Res.*, 78:2885–2906, 1973.

[15] A. I. Eriksson, M. André, B. Klecker, H. Laakso, P.-A. Lindqvist, F. Mozer, G. Paschmann, A. Pedersen, J. Quinn, R. Torbert, K. Torkar, and H. Vaith. Electric field measurements on Cluster: comparing the double-probe and electron drift techniques. *Ann. Geophysicae*, 24:275–289, 2006.

[16] E. Engwall, A. I. Eriksson, M. André, I. Dandouras, G. Paschmann, J. Quinn, and K. Torkar. Low-energy (order 10 ev) ion flow in the magnetotail lobes inferred from spacecraft wake observations. *Geophys. Res. Lett.*, 33:L06110, doi:10.1029/2005GL025179, 2006.

[17] B. Feuerbacher and B. Fitton. Experimental investigation of photoemission from satellite surface materi-

als. *J. Appl. Phys.*, 43:1563–1572, 1972.

[18] G. Gustafsson, R. Boström, B. Holback, G. Holmgren, A. Lundgren, K. Stasiewicz, L. Ahlén, F. S. Mozer, D. Pankow, P. Harvey, P. Berg, R. Ulrich, A. Pedersen, R. Schmidt, A. Butler, A. W. C. Fransen, D. Klinge, M. Thomsen, C.-G. Fälthammar, P.-A. Lindqvist, S. Christenson, J. Holtet, B. Lybekk, T. A. Sten, P. Tanskanen, K. Lappalainen, and J. Wygant. The electric field and wave experiment for the Cluster mission. *Space. Sci. Rev.*, 79:137–156, 1997.

[19] C. P. Escoubet, M. Fehringer, and M. Goldstein. The Cluster mission. *Ann. Geophysicae*, 19:1197–1200, 2001.

[20] E. Winkler. Plasma densities and satellite potentials: A study of the EUV interaction with the Cluster spacecrafts. Master thesis, Swedish Institute of Space Physics, Uppsala, and Department of Astronomy and Space Physics, Uppsala University, 2007.

[21] T. N. Woods, F. G. Eparvier, S. M. Bailey, P. C. Chamberlin, J. Lean, G. J. Rottman, S. C. Solomon, W. K. Tobiska, and D. L. Woodraska. Solar EUV experiment (SEE): Mission overview and first results. *J. Geophys. Res.*, 110:A01312, doi:10.1029/2004JA010765, 2005.

[22] J. A. R. Samson and R. B. Cairns. Photoelectric yield of aluminum from 300 to 1300 A. *Rev. Sci. Instr.*, 36:19–21, 1965.

[23] C. L. Lawson and R. J. Hanson. *Solving least squares problems*. SIAM, 1974.

[24] H. Rème *et al.* The Cluster Ion Spectrometry (CIS) Experiment. *Space Sci. Rev.*, 79:303–350, January 1997.

[25] H. Rème et al. First multispacecraft ion measurements in and near the Earth's magnetosphere with the identical Cluster ion spectrometry (CIS) experiment. *Ann. Geophysicae*, 19:1303–1354, 2001.

[26] P. W. Daly. Users guide to the Cluster science data system. Technical Report DS-MPA-TN-0015 (http://sci2.estec.esa.nl/cluster/csds/csds.html), Max-Planck-Institut für Aeronomie, Lindau, Germany, 2002.

[27] T. N. Woods, W. K. Tobiska, G. J. Rottman, and J. R. Worden. Improved solar Lyman α irradiance modelling from 1947 through 1999 based on UARS observations. *J. Geophys. Res.*, 105:27195–27215, 2000.

[28] W. K. Tobiska. Validating the solar EUV proxy, E10.7. *J. Geophys. Res.*, 106:29969–29978, 2001.

[29] L. H. Brace, W. R. Hoegy, and R. F. Theis. Solar EUV measurements at Venus based on photoelectron emission from the Pioneer Venus Langmuir probe. *J. Geophys. Res.*, 93:7282–7296, 1988.

[30] K. K. Mahajan, H. O. Upadhyay, N. K. Sethi, W. R. Hoegy, W. D. Pesnell, and L. H. Brace. Pioneer Venus orbiter measurements of solar EUV flux during solar cycles 21 and 22. *Solar Phys.*, 177:203–216, 1998.